JCTC Journal of Chemical Theory and Computation

Article

pubs.acs.org/JCTC

Understanding Electronically Non-Adiabatic Relaxation Dynamics in Singlet Fission

Guohua Tao*

Shenzhen Key Laboratory of New Energy Materials by Design, Peking University, Shenzhen 518055, China

School of Advanced Materials, Peking University Shenzhen Graduate School, Shenzhen 518055, China

Supporting Information

ABSTRACT: Nonadiabatic relaxation of one singlet state into two triplet states is the key step in singlet fission dynamics, the understandings of which may help design next generation solar cells. In this work we perform the symmetrical quasi-classical (SQC) nonadiabatic molecular dynamics (MD) simulation [Cotton and Miller, *J. Phys. Chem. A*, **2013**, *117*, 7190; Meyer and Miller, *J. Chem. Phys.* **1979**, *70*, 3214] for a model system to study the real-time fission dynamics. The dependence of the nonadiabatic relaxation dynamics on energy levels, electronic couplings, and electronic-phonon couplings has been examined, in comparison with other analytical approximations, such as Förster theory and Marcus theory. Unlike many other methods, the SQC nondiabatic MD simulation approach is able to describe fission dynamics efficiently and accurately enough to provide microscopic insights into singlet fission.

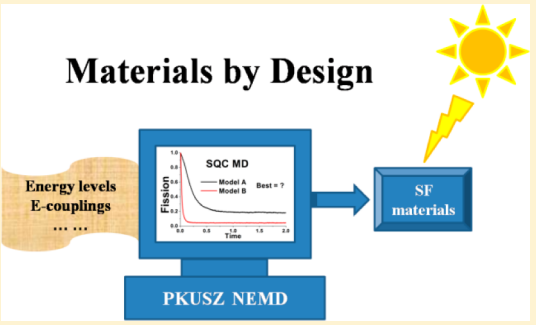

I. INTRODUCTION

Singlet fission (SF) in organic semiconductors, involving nonadiabatic relaxation of a singlet state (S1) into two triplet states (T+T) or a correlated triplet pair (TT), inspires new ideas on maximizing the photoelectric conversion in developing highly efficient organic solar cells.[1,2] SF dynamics is inherently an ultrafast nonadiabatic relaxation process, which occurs on the time scale of tens femtoseconds to picoseconds. Furthermore, electronic couplings and electronic−phonon couplings are very complicated, and both mediate fission dynamics significantly. The complexity in both time and spatial domains obscures the microscopic mechanisms of singlet fission and presents great challenges to researchers, from both experimental and theoretical aspects. Nevertheless, it is now feasible to identify singlet, triplets, and intermediate multi-excitation states[3−6] (or doubly excited exciton, i.e., TT) from state-of-the-art ultrafast transient experiments. Theoretically, ab initio quantum mechanical calculations, such as density functional theory,[7] multireference CAS-MP2,[8] and many body perturbation theory,[9−11] make it possible to estimate energy levels and electronic couplings. For example the role of the TT state in SF dynamics was conjectured early by Kuhlman et al.[7] and Zimmerman et al.[8] Due to spectral overlap and the unknown optical transitions, detailed spectroscopic assignments are very difficult and the proposals for the photophysics of SF are often controversial.[1] On the other hand, ab intio quantum mechanical calculations for complex molecular systems suffer from large errors,[2] especially as the system size increases, not to mention true molecular dynamics simulations.

However, there is little doubt that a comprehensive understanding of SF mechanisms relies on a fully dynamical treatment at a microscopic molecular level. For example, the S1 excition decay time in pentacene from direct time-resolved measurements spans from 70 to 200 fs,[3,5,12−14] but the underlying molecular mechanism is unclear. Zimmerman and co-workers[15] proposed that SF proceeds through a direct pathway from the S1 to the TT state, and nonadiabatic transitions induced by intermolecular interactions account for the subpicosecond decay time. By contrast Zhu and co-workers conducted time-resolved two-photon photoemission (TR-2PPE) spectroscopy experiments in crystalline pentacene[3] and tetracene,[4] claimed that SF dynamics is quantum coherent and occurs through a CT mediated pathway.[16] There is also a possibility that the direct pathway and the CT mediated pathway coexist and pathway interference controls the dynamics quantum mechanically.[17]

Energy levels, electronic couplings, electron−phonon couplings are all essential elements in constructing a global picture of SF, which would be extremely useful to the rational design of new materials. It is therefore worthwhile to study how exactly these factors mediate dynamics microscopically.

The setting of energy levels is one of the most important factors in designing new efficient SF chromophores.[18,19] Energetically SF needs to be slightly exoergic or isoergic to achieve high efficiency and to compete with other processes such as fluorescence. In an early work based on a phenomenological density matrix model,[18] Greyson et al. suggested that high fission yield requires the change in free energy as close to zero as possible, at least for coherent

Received: October 27, 2014
Published: December 8, 2014

dynamics without dephasing and at zero temperature, and energy levels should be paid more attention than electronic couplings in chromophore design. When considering thermal energy and coherent excitation, slight endothemicity is also tolerable. Indeed, Teichen and Eaves demonstrated that the solvent-induced fluctuations in energy levels of chromophores are able to promote SF.[19] Prezhdo and co-workers actually observed the phonon-induced fluctuations in the state energies in their ab initio nonadiabatic MD simulations.[20,21] Apparently bath effect should also be part of the design principle for maximizing SF yield. Reichman and co-workers investigated the bath effect in SF in the framework of Redfield theory,[16,22,23] and their results indicated that fission is largely insensitive to temperature[16] or different bath relaxation functions.[22]

Another key element in SF materials design is electronic couplings. The SF rate is directly related to electronic couplings, which contains contributions from either the first order direct coupling or higher order mediated interactions, or both. In the superexchange mechanism[22,23] [i.e., $E(\mathrm{CT}) > E(\mathrm{S1}) > E(\mathrm{TT})$], the fission rate is predicted to follow a forth order scaling with respect to the electronic coupling elements. A relatively large electronic coupling (330 meV) is also estimated in a pentacence system to account for quantum coherence observed in fission dynamics.[3]

There are a number of approximated theoretical methods to be applied in describing SF dynamics, such as Förster theory[24] (and Marcus theory[25] for SF), Redfield theory, reduced hierarchy equation approach,[23,26] multiconfiguration time-dependent Hartree (MCTDH) method,[27,28] and mixed quantum-classical technique based on time domain DFT[29] and surface hopping.[30] Their successes and disadvantages are discussed in ref 17. Of the most relevant to this work, Förster theory is good for the weak electronic coupling limit, and in some cases it even predicts the energy transfer rate qualitatively well in a wide range of reorganization energy.[26] However, the incoherent Förster theory (or Marcus theory) is unable to describe electronic coherence correctly and favors the sequential mechanism [i.e., $E(\mathrm{S1}) > E(\mathrm{CT}) > E(\mathrm{TT})$] over the superexchange one.[19] By contrast, Redfield theory treats electronic couplings accurately, which predicts an efficient superexchange mediated fission mechanism,[22,23] going beyond the design rules based on the early static calculations[15] or Förster theory.[19] However, Redfield theory makes perturbations on electronic−phonon couplings therefore breaks down in the strong electronic−phonon coupling regime. For example, the secular, Markovian Redfield theory, predicts a wrong linear dependence of fission rate on the reorganization energy in the entire region.[22]

To describe the nonadiabatic relaxation of SF dynamics, it is essential to treat electronic−nuclear couplings and coherence accurately. To proceed, Meyer and Miller[31] proposed a quantum mechanically exact model many years ago, in which electronic degrees of freedom (DOFs) are mapped into classical variables and therefore the electronically nonadiabatic MD simulations can be performed accurately in a dynamically consistent way for all DOFs. The Meyer−Miller (MM) model has been implemented to nonadiabatic molecular dynamics with a great success in a variety of interesting applications.[32] Since the fully quantum mechanical description is apparently inapplicable for complex molecular systems, recently Cotton and Miller developed an extremely efficient symmetrical quasi-classical (SQC) nonadiabatic MD simulation approach[33−35] based on the MM model. Apart from its simplicity, it has been shown that the SQC method produces excellent agreement with exact quantum mechanical results[33−35] and is capable of providing physical insights into molecular mechanisms in a variety of important electronically nonadiabatic problems, including state-to-state reactive scattering,[33] electronically nonadiabatic dynamics in the spin-boson systems,[34] electron transfer and proton coupled electron transfer[35] and quantum dynamics and pathway interference in SF.[17,36]

In separate work,[36] we systematically examined the dependence of fission dynamics on some key factors in the bath modeling by applying the SQC method to a model system of pentacene. Not surprisingly, the results show that fission dynamics depends on characteristic frequencies or reorganization energy much more than the functional form of spectra density or bath temperatures. However, the detailed mechanisms can only be revealed by real time dynamical simulations. For example, the SQC results clearly demonstrated that the temperature independence in the nonadiabatic relaxation of S1 is largely due to the thermally inactive bath modes instead of the electronic energy barrier, which would provide microscopic explanations to the experimental measurements.

In this work, we study fission dynamics by using the SQC method and focus on the dependence of fission rate on energy levels, electronic couplings, and some features in the bath modeling. We evaluate the fission rates and make comparisons between the SQC results with those obtained from other analytic approximations based on perturbation theory and/or rate equations. Section II briefly describes the theoretical methods and models. Results and discussions are presented in Section III. Section IV concludes.

II. THEORETICAL METHOD AND MODELS

a. Nonadiabatic Molecular Dynamics Simulation. The classical Meyer−Miller Hamiltonian used in electronically nonadiabatic MD simulations takes the following form:[31,32]

$$H(\mathbf{x}, \mathbf{p}, \mathbf{Q}, \mathbf{P}) = \sum_{k=1}^{n}\left(\frac{1}{2}x_k^2 + \frac{1}{2}p_k^2 - \gamma\right)H_{kk}(\mathbf{Q}, \mathbf{P}) + \sum_{k=1}^{n}\sum_{l=k+1}^{n}(x_k x_l + p_k p_l)H_{kl}(\mathbf{Q}, \mathbf{P}) \quad (1)$$

where H_{kk} and H_{kl} are the diagonal and off-diagonal Hamiltonian matrix elements. $(\mathbf{x},\mathbf{p})$ and $(\mathbf{Q},\mathbf{P})$ are the phase points for the classical electronic and nuclear degrees of freedom (DOFs), respectively. $n_k = {}^1/_2(x_k^2 + p_k^2) - \gamma$ and $x_k x_l + p_k p$ are the population and coherence of the electronic state k, respectively, and γ is a parameter accounting for the effective zero point energy.[33]

Dynamical properties can be evaluated by the statistical ensemble average of the corresponding time-dependent variable, formally exact the same way as that is done in classical MD simulations:

$$A(t) = \frac{1}{(2\pi\hbar)^{2N+2n}}\int \mathrm{d}\mathbf{x}_0\mathrm{d}\mathbf{p}_0\mathrm{d}\mathbf{Q}_0\mathrm{d}\mathbf{P}_0 A(\mathbf{x}_t, \mathbf{p}_t, \mathbf{Q}_t, \mathbf{P}_t)\rho(\mathbf{x}_0, \mathbf{p}_0, \mathbf{Q}_0, \mathbf{P}_0) \quad (2)$$

where N, and n are the nuclear and electronic DOFs, respectively; $\rho(\mathbf{x}_0,\mathbf{p}_0,\mathbf{Q}_0,\mathbf{P}_0)$ is the probability distribution function depending on initial conditions.

A very efficient way to compute eq 2 is the symmetrical quasi classical (SQC) approach recently developed by Cotton and

dx.doi.org/10.1021/ct500953r | J. Chem. Theory Comput. 2015, 11, 28−36

Miller,[33] in which a symmetrical binning window function is applied to project the ensemble of quasi-classical trajectories onto the corresponding electronic state, that is,

$$W_k(n_k, N) = \frac{1}{\Delta n} h\left(\frac{\Delta n}{2} - |n_k - N|\right) \tag{3}$$

where $h(z)$ is the Heaviside function, $\Delta n = 2\gamma$, and N (0 or 1) is the electronic quantum number indicating the electronic state is occupied or not. More details can be found in ref 33. Without loss of generality, assuming the system starts from the state i, the SQC time-dependent electronic population of state k can be evaluated from a Monte Carlo averaging procedure:

$$P_k(t) = \{\langle W_i(n_i(0), 1) \prod_{l\neq i}^{n} W_l(n_l(0), 0) W_k(n_k(t), 1) \prod_{l\neq k}^{n} W_l(n_l(t), 0)\rangle\} / \{\prod_{k}^{n} \langle W_i(n_i(0), 1) \prod_{l\neq i}^{n} W_l(n_l(0), 0) W_k(n_k(t), 1) \prod_{l\neq k}^{n} W_l(n_l(t), 0)\rangle\} \tag{4}$$

b. Rate Theory. The time-dependent electronic populations may also be determined by quantum master equation[19]

$$\frac{dP_j(t)}{dt} = -\int_0^t ds \sum_k R_{j,k}(s) P_k(t - s) + I_j(t) \tag{5a}$$

where $R_{j,k}(s)$ is the relaxation operator and $I_j(t)$ the quantum inhomogeneous term that depends on the initial conditions. Replacing $P_k(t - s)$ by $P_k(t)$, we obtain the Markovian quantum Master equation

$$\frac{dP_j(t)}{dt} = -\sum_k K_{j,k}(t) P_k(t) \tag{5b}$$

Here, we also assume the initial density matrix is diagonal, therefore the second term in the right-hand side of eq 5a drops out, that is, $I_j(t) = 0$.

Applying the second order perturbation theory on the electronic coupling, the weak coupling limit of eq 5 is

$$\frac{dP_j(t)}{dt} = \sum_k [W_{k\to j}(t) P_k(t) - W_{j\to k}(t) P_j(t)] \tag{6}$$

and the rate constant is a non-Markovian generation of Fermi's golden rule

$$W_{j\to k}(t) = 2V_{jk}^2 \int_0^t d\tau \mathrm{Re}[Tr_B\{e^{-iH_k\tau} e^{iH_j\tau} \rho_j(t)\}] \tag{7}$$

where $\rho_j(t)$ is time-dependent density function of state j. Once making Markovian approximation, that is, $t \to \infty$, eq 7 turns into Fermi's golden rule

$$W_{j\to k} = 2V_{jk}^2 \int_0^\infty d\tau \mathrm{Re}[\langle e^{-iH_k\tau} e^{iH_j\tau}\rangle_j] \tag{8}$$

where $\langle A\rangle_j = \mathrm{Tr}_B[A\rho_j^{eq}]$ is the equilibrium ensemble average of the operator A with respect to the state j, and $\rho_j^{eq} = \exp(\beta H_j)/\mathrm{Tr}_B[\exp(\beta H_j)]$. By taking advantage of the cumulant expansion technique, we recover Förster theory's result for the incoherent hopping rate

$$W_{j\to k} = \frac{V_{jk}^2}{2\pi} \int_{-\infty}^{\infty} d\omega A_k(\omega) F_j(\omega) \tag{9a}$$

where

$$A_k(\omega) = \int_{-\infty}^{\infty} dt e^{i\omega t} e^{-i(E_k+\lambda_k)t - g_k(t)} \tag{9b}$$

and

$$F_j(\omega) = \int_{-\infty}^{\infty} dt e^{i\omega t} e^{-i(E_j-\lambda_j)t - g_j^*(t)} \tag{9c}$$

are the absorption and fluorescence spectrum. $g(t)$ is the line shape function determined by the spectra density $J(\omega)$

$$g_k(t) = \frac{1}{\pi} \int_0^\infty d\omega \frac{J_k(\omega)}{\omega^2} \left[\coth\left(\frac{\beta\omega}{2}\right)(1 - \cos\omega t) - i(\omega t - \sin(\omega t))\right] \tag{9d}$$

In the high temperature limit and the short time (static environment or slow modulation) limit, that is, $k_B T \gg \hbar\omega$ and $\omega t \to 0$, $g(t) \approx \lambda k_B T t^2$, the rate is given by

$$W_{j\to k} = V_{jk}^2 \sqrt{\frac{\pi}{2\lambda k_B T}} \exp\left[-\frac{(E_k - E_j + 2\lambda)^2}{8\lambda k_B T}\right] \tag{10}$$

which is Marcus theory's result for the singlet fission rate. Here, E_j is the energy of state j, V_{jk} is the (effective) electronic coupling between state j and k, and 2λ is the reorganization energy for the energy transfer case (note the $\lambda = \pi^{-1}\int d\omega J(\omega)/\omega$ is the reorganization energy for electron transfer processes).[19]

c. Model System. We take the three-state model[17] for pentacene as an example to study the nonadiabatic relaxation dynamics in SF, that is,

$$S1 \underset{k-1}{\overset{k1}{\rightleftharpoons}} C \underset{k-2}{\overset{k2}{\rightleftharpoons}} TT \tag{11}$$

The Hamiltonian is the same as that in our previous work,[17] which includes three parts: electronic, phonon, and electronic−phonon couplings,

$$H = H_{el} + H_{ph} + H_{el-ph} \tag{12}$$

with $H_{el} = \Sigma_{k=1}^{n} |k\rangle E_k \langle k| + \Sigma_{l\neq k} |k\rangle E_{kl} \langle l|$, $H_{ph} = \Sigma_{k=1}^{n} \Sigma_j^{N_b} [((P_{kj}^2)/2) + (1/2)\omega_{kj}^2 Q_{kj}^2]$ and $H_{el-ph} = \Sigma_{k=1}^{n} |k\rangle\langle k| \Sigma_j (- c_{kj} Q_{kj})$. Here, (Q_{kj}, P_{kj}) is the phase space point of the j-th bath mode coupled with the k-th electronic state, with ω_{kj}, c_{kj} the frequency and the coupling constant, respectively, and N_b is the number of the bath modes coupled with each single electronic state.

From eqs 9 and 10, it is obvious that energy levels, electronic couplings, and electronic−phonon couplings play an important role in determining fission rate. In this work, we consider several different settings for the energy levels, which are listed in Table 1. The first model, that is, the Model A in ref 17, consists of an exothermal pathway with an energy barrier (the intermediate CT state). The energy levels of the initial and the final state are the same in the first three models, while Model 2 is a straight downhill pathway and Model 3 has a higher barrier.

Table 1. Energy Levels for Different Models Used in This Work (meV)

	Model 1	Model 2	Model 3	Model 4	Model 5
E(S1)	200	200	200	100	0
E(CT)	300	100	500	300	300
E(TT)	0	0	0	0	200

dx.doi.org/10.1021/ct500953r | J. Chem. Theory Comput. 2015, 11, 28−36

In comparison with Model 1, Model 4 lifts up the level of S1, and Model 5 reverses the pathway direction in Model 1, which was taken to model tetracene in prior work.[17]

The electronic−phonon interactions are determined by the spectra density of phonon bath modes, that is,

$$J(\omega) = \frac{\pi}{2}\sum_k \frac{c_k^2}{\omega_k}\delta(\omega - \omega_k) \tag{13a}$$

Since SF dynamics is largely independent of the functional form of the spectra density, in this work we consider mainly the Debye bath, that is,

$$J(\omega) = \frac{2\lambda\omega\omega_c}{\omega^2 + \omega_c^2} \tag{13b}$$

Here, λ is the reorganization energy, and ω_c is the characteristic frequency of the bath. The high frequency bath (ω_c = 180 meV) is used to model the spectra density in conjugated organic molecules. A low frequency bath (ω_c = 5 meV) is also considered for comparison. We discretize the continuous spectra density in the same way suggested by Wang et al.[37] See our previous work for more details.[17,36]

d. Electronic Couplings. As shown in eq 7, the Golden Rule rate depends on the square of the electronic coupling between the initial and the final state. When there is an intermediated CT state involved, the effective electronic coupling includes high order contributions.[1,22] The first order perturbation approximation to the CT coupled S1 excited state is given by

$$|\mathrm{S1}^{(1)}\rangle = |\mathrm{S1}^{(0)}\rangle + \frac{V(\mathrm{S1}-\mathrm{CT})}{E(\mathrm{S1}) - E(\mathrm{CT})}|\mathrm{CT}\rangle \tag{14a}$$

and similar for the TT state

$$|\mathrm{TT}^{(1)}\rangle = |\mathrm{TT}^{(0)}\rangle + \frac{V(\mathrm{CT}-\mathrm{TT})}{E(\mathrm{TT}) - E(\mathrm{CT})}|\mathrm{CT}\rangle \tag{14b}$$

So the electronic coupling between the S1 and the TT state is given by

$$\begin{aligned} V_{\mathrm{S1-TT}} \equiv \langle \mathrm{S1}|V_{\mathrm{el}}|\mathrm{TT}\rangle &\approx \langle \mathrm{S1}^{(0)}|H_{\mathrm{el}}|\mathrm{TT}^{(0)}\rangle + \frac{V(\mathrm{S1}-\mathrm{CT})V(\mathrm{CT}-\mathrm{TT})}{E(\mathrm{TT}) - E(CT)} \\ &+ \frac{V(\mathrm{S1}-\mathrm{CT})V(\mathrm{CT}-\mathrm{TT})}{E(\mathrm{S1}) - E(\mathrm{CT})} = V(\mathrm{S1}-\mathrm{TT}) \\ &+ \frac{V(\mathrm{S1}-\mathrm{CT})V(\mathrm{CT}-\mathrm{TT})[E(\mathrm{S1}) + E(\mathrm{TT}) - 2E(\mathrm{CT})]}{[E(\mathrm{S1}) - E(\mathrm{CT})][E(\mathrm{TT}) - E(\mathrm{CT})]} \end{aligned} \tag{15}$$

Here, the first term is the direct coupling, and the second one is the contribution from the intermediate pathway. Since the rate is proportional to the square of the total coupling, eq 15 (together with eq 9 or eq 10) clearly explains the existence of quantum interference between the direct and the intermediate pathway. By contrast, the rate equation eq 19 (see below) is a classical superposition of individual pathways and thus cannot describe the pathway interference.

e. Kinetic Rate Equation. To estimate the fission rate, we assume the following rate equations for the CT mediated pathway, in line with eq 6:

$$\begin{aligned} \frac{\mathrm{d}}{\mathrm{d}t}[\mathrm{S1}] &= -k_1[\mathrm{S1}] + k_{-1}[CT] \\ \frac{\mathrm{d}}{\mathrm{d}t}[\mathrm{CT}] &= k_1[\mathrm{S1}] + k_2[TT] - k_{-1}[\mathrm{CT}] - k_2[\mathrm{CT}] \\ \frac{\mathrm{d}}{\mathrm{d}t}[\mathrm{TT}] &= k_2[\mathrm{CT}] - k_{-2}[\mathrm{TT}] \end{aligned} \tag{16}$$

By making the steady state approximation, we obtain the decay rate of the S1 population,

$$k_{12} = \frac{k_1k_{-1}(k_2 + k_{-2}) + k_2k_{-2}(k_1 + k_{-1}) + k_1k_2^2 + k_{-1}^2k_2}{(k_{-1} + k_2)\,(k_{-1} + k_2 + k_{-2})} \tag{17}$$

Some special cases are interesting. (1) High barrier case: that is, $k_{-1} \sim k_2 \gg k_1 \sim k_{-2}$, (ex. Model 1, and Model 3), then $k_{12} \approx ((k_1k_{-1}(k_2 + k_{-2}) + k_2k_{-2}(k_1 + k_{-1}) + k_1k_2^2 + k_{-1}^2k_2)/((k_{-1} + k_2)^2))$ is symmetric with respect to the direction of fission dynamics. As an example the rate calculated by using eq 17 with either Förster theory or Marcus theory for Model 5 is almost identical to that for Model 1. (2) Downhill case: that is, $k_1 \sim k_2 \gg k_{-1} \sim k_{-2}$, (ex. Model 2), then $k_{12} \approx k_1$.

When the direct pathway opens up, i.e. the direct coupling of the S1 and the TT state is nonzero, a slight modification is needed on the rate expression in eq 16, and another two terms associated with the direct pathway should be added in, that is,

$$\begin{aligned} \frac{\mathrm{d}}{\mathrm{d}t}[\mathrm{S1}] &= -k_1[\mathrm{S1}] + k_{-1}[\mathrm{CT}] - k_3[\mathrm{S1}] + k_{-3}[\mathrm{TT}] \\ \frac{\mathrm{d}}{\mathrm{d}t}[\mathrm{CT}] &= k_1[\mathrm{S1}] + k_2[\mathrm{TT}] - k_{-1}[\mathrm{CT}] - k_2[\mathrm{CT}] \\ \frac{\mathrm{d}}{\mathrm{d}t}[\mathrm{TT}] &= k_2[\mathrm{CT}] - k_{-2}[\mathrm{TT}] + k_3[\mathrm{S1}] - k_{-3}[\mathrm{TT}] \end{aligned} \tag{18}$$

The overall rate thus can be calculated as the follows:

$$k_{13} = k_{12} + k_3 + k_{-3}\frac{k_1 + k_{-1} + k_2}{k_{-1} + k_2 + k_{-2}} \tag{19}$$

where k_{12} is given by eq 17. Equation 19 reduces to eq 17 when $k_3 = k_{-3} = 0$, as it should be.

III. RESULTS AND DISCUSSION

a. Rate in Various Models and Bath Effect. First we consider the CT mediated pathway [i.e., V(S1-TT) = 0] for Model 1, namely E(S1)-E(TT) = 200 meV, E(CT)-E(TT) = 300 meV, and V(S1-CT) = V(CT-TT) = −50 meV; T = 300 K and ω_c = 180 meV. We calculated the state−state transition rate (normalized by the square of the electronic coupling) [see Figure 1a−d] by using Förster theory (eq 9), and Marcus theory (eq 10). The overall fission rate is obtained by the kinetic rate equation model eq 16, and shown in Figure 1 e and f, together with the rate calculated by using eq 10 for the overall S1-TT transition (i.e., j = S1, k = TT; labeled as Marcus II) and by fitting to the real-time SQC dynamics. The fitting model we used is a two exponential decay function:

$$P(\mathrm{S1}) = A\,\exp(-t/\tau_1) + (1 - A)\exp(-t/\tau_2) \tag{20}$$

and the first time constant is taken as the stationary rate, that is, $k_{\mathrm{SF}} = 1/\tau_1$ (except where noted below).

The agreement between Förster theory and SQC simulations is pretty good. Marcus theory, instead, predicts a severe

dx.doi.org/10.1021/ct500953r | J. Chem. Theory Comput. 2015, 11, 28−36

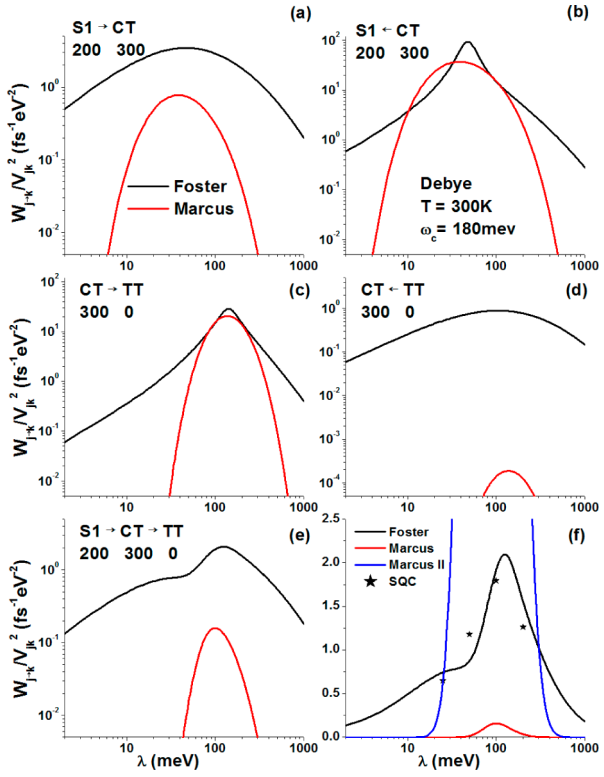

Figure 1. Rate from state $|j\rangle$ to $|k\rangle$ as a function of the reorganization energy λ. Results are calculated by Förster theory eq 9 (black), by Marcus theory eq 10 (red), for the initial and final states specified in the legends, and by eq 10 for j = S1, k = TT (blue). The overall rate is obtained by using eq 16 [lines in e and f, note the normal scale in y axis in f] and by the fitting to the SQC simulation results via eq 20 [stars in f]. Model 1 with high frequency bath (ω_c = 180 meV).

underestimate on the uphill transfer rate and the overall rate. In the downhill cases (Figure 1b and c), Marcus rate is comparable with Förster rate around the maximum but fall off exponentially as the electronic−phonon coupling increases or decreases. This is not surprising since Marcus theory is the high temperature and static environment limit of eq 9, and here, T = 26 meV ≪ ω_c = 180 meV. Marcus II does provide a better prediction in some cases. However, the overall agreement with the SQC nonaidabatic simulation results is still poor. The comparison of decay times is shown in Table 2. For Marcus II, we assume that the effective S1-TT coupling $V_{S1\text{-}TT}$ = −50 meV here. The effective coupling $V_{S1\text{-}TT}$ may also be evaluated by eq 15, and applied to the overall S1-TT transition rate calculations by specifying the initial and final states as j = S1, k = TT in Förster (labeled as Forster #) or Marcus theory (labeled as Marcus #). These results are also listed in Table 2. It is clear that (1) treating the CT intermediated state implicitly as a perturbation to the direct pathway does not guarantee a better prediction for the overall rate, but sometimes, it is an even worse choice (Förster) and (2) taking other values of $V_{S1\text{-}TT}$ would be equivalent to a uniform rescaling of the rate, which makes no further improvements.

For comparison, we examine fission dynamics coupled with the low characteristic frequency bath (ω_c = 5 meV). In this case, the high temperature and slow modulation limit approximation is more satisfied, and indeed, the rates predicted by Marcus theory are getting closer to Förster theory's results.

Table 2. Rate (in ps) as a Function of Reorganization Energy λ (in meV) for Model 1 [T = 300 K with V(S1-TT) = 0][a]

	λ (meV)			
	25	50	100	200
high frequency bath (ω_c = 180 meV)				
SQC	**0.619**	**0.339**	**0.223**	**0.317**
Förster	**0.538**	**0.456**	**0.208**	**0.256**
Förster #	0.290	0.0867	0.0211	0.106
Marcus	6.90×10^4	26.8	2.52	11.1
Marcus II	0.630	0.0302	0.0162	0.0604
Marcus #	1.42	0.0679	0.0365	0.136
low frequency bath (ω_c = 5 meV)				
SQC	**11.2(0.003)***	**1.36**	**0.597**	**3.85(0.293)***
Förster	**17.4**	**6.02**	**1.07**	**2.68**
Förster #	0.694	0.0454	0.0245	0.0887

[a]*We take the second time constant which represents the majority of population since a very short-time decay (shown in parentheses) is involved. Marcus (Marcus II and Marcus #) results are independent of bath frequency.

Note Marcus theory (and Marcus II) is independent of spectra density, so these results are the same in Figures 1 and 2. Still,

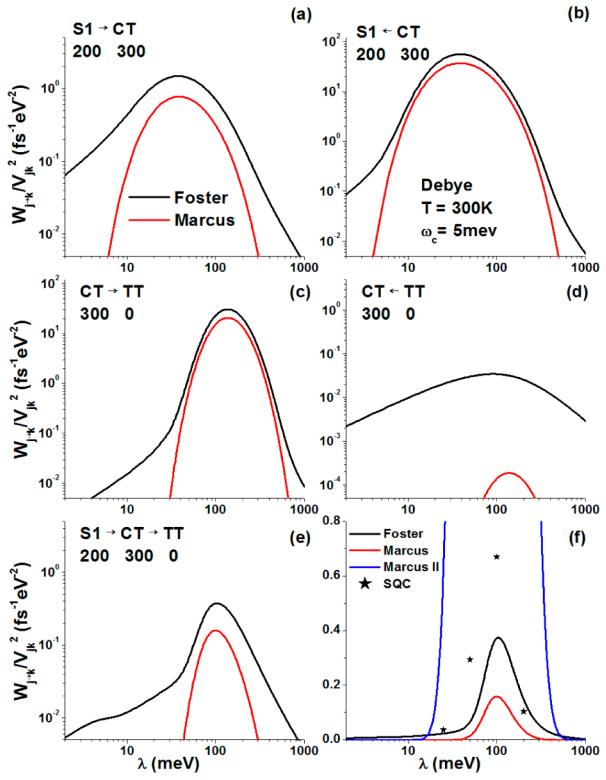

Figure 2. Same as in Figure 1 except for low frequency bath (ω_c = 5 meV).

Förster theory makes much better predictions on rate than Marcus theory. We also consider the nonadiabatic fission dynamics coupled with Ohmic bath, that is, $J(\omega) = \eta\omega\, e^{-\omega/\omega_c}$. The results are similar to those shown here for Debye bath (see Supporting Information Figure S1).

Now we examine the dependence of the rate on energy levels, as a function of the reorganization energy. Without loss of generality, we consider the system coupled with a high frequency Debye phonon bath at room temperature. The

dx.doi.org/10.1021/ct500953r | J. Chem. Theory Comput. 2015, 11, 28−36

results for Model 1 have been shown in Figure 1f, and those for other models in Table 1 are shown in Figure 3. Changes in the

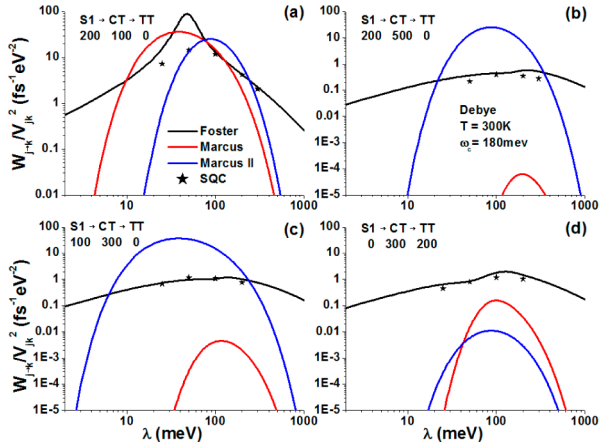

Figure 3. Rate in various models as a function of the reorganization energy λ. Debye bath ω_c = 180 meV, and T = 300 K.

energy level of the intermediate CT state significantly alter the fission rate [see Figure 4a (the same as Figure 1 f but in log–

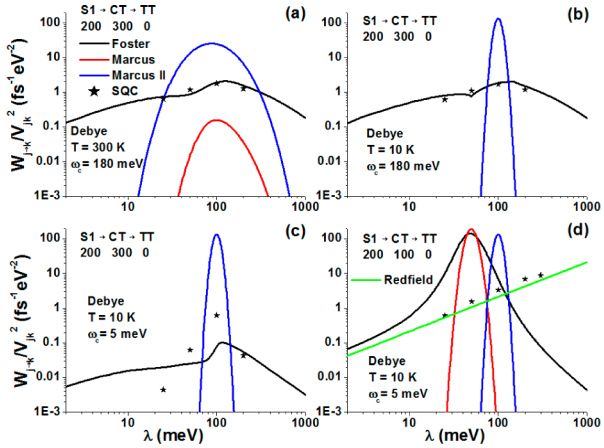

Figure 4. Rate at low temperature as a function of the reorganization energy λ. Debye bath, T = 10 K. (a) Results for T = 300 K and ω_c = 180 meV for comparison; (b) ω_c = 180 meV; (c) ω_c = 5 meV; (d) ω_c = 5 meV, Model 2. Marcus results are too small to show in panels b and c.

log scale), Figure 3a and b]. Förster theory predicts rates in good agreement with the SQC results, even though a way off from a quantitative description of fission dynamics. Marcus theory reflects the change of the intermediate level in the energy diagram, but sometimes it predicts a rate with an error of several orders of magnitude, ex. Models 3 and 4 (Figure 3b and c). Marcus II does not show explicit dependence on the intermediate CT state, which predicts exactly the same rate for model 1, 2, and 3 (note the different scales in Figure 3a and b, Figure 4a). It performs better in some cases (ex. Figure 3b and c), worse in others (ex. Figure 3d), than the faithful three-state Marcus treatment. None of them seems to work well globally in the reorganization energy space.

The maximum of the state–state transition rate predicted by Marcus theory (eq 10) locates around the reorganization energy $\lambda \sim -(\Delta E/2) = ((E_j - E_k)/2)$ (actually smaller due to the prefactor). The maximum of the overall rate is therefore determined by the combination of the corresponding state–state rates. For example in Model 1, k_1 and k_{-1} reach their maxima around $\lambda \sim 40$ meV, the maxima of k_2 and k_{-2} are around $\lambda \sim 140$ meV, and the maximum of the overall rate (calculated from eq 17) appears around $\lambda \sim 90$ meV, which coincides with that obtained by the Marcus II result (see Figures 1 and 4a). In general, these two treatments predict quite different rates, not only in the magnitude but in the location of maximum (see Figure 3).

In prior work,[36] fission dynamics is shown almost temperature independent for the high frequency bath cases, while noticeable temperature dependence is observed for the low frequency bath cases. Here, we examine how different rate theory works in the low temperature region (see Figure 4, the corresponding high-temperature results also shown for comparison). Förster theory works pretty well for high frequency bath (Figure 4a and b) but becomes unsatisfactory for low frequency bath (Figure 4c and d). Marcus theory with rate equations underestimates the rate too much, and the results even fall outside the plotted regions in Figure 4b and c. Marcus II works well in a small region around the maximum but becomes bad quickly outside that region.

In a different setting of energy diagram (Model 2, Figure 4d), there are considerable deviations in the rate prediction for the low frequency bath at low temperature between the above-mentioned analytic approximations and the SQC nonadiabatic simulations. One may argue that the discrepancy could attributes to (1) errors in the numerical fitting to the SQC results, and (2) the steady state approximation in the rate equations. However, it seems unlikely true since they do not appear to be significant enough to destroy the nice agreement between Förster theory and SQC simulations in the high temperature, high frequency bath cases (see Figures 3 and 4), or between Redfield theory and SQC simulations in the low temperature, low frequency bath case for Model 2 (see Figure 4d). Actually the SQC approach predicts a nearly linear dependence with respect to the reorganization energy, in excellent agreement with the secular Redfield theory. The Redfield rate is given by[22]

$$k_{\alpha\beta} = \hbar^{-1} C_{\alpha\beta} J(\omega_{\alpha\beta})[n_{\mathrm{BE}}(\omega_{\alpha\beta}) + 1] \tag{21}$$

where $C_{\alpha\beta} = 2\Sigma_i |\langle\alpha|i\rangle|^2 |\langle\beta|i\rangle|^2$, $\omega_{\alpha\beta} = |E_\alpha - E_\beta|/\hbar$, $n_{\mathrm{BE}}(\omega) = 1/(e^{\hbar\omega/K_B T} - 1)$, and $J(\omega)$ is the spectra density. This case clearly exemplifies the breakdowns of Förster theory or Marcus theory in the rate prediction.

b. Electronic Couplings and Pathway Interference. In the following we investigate the role of electronic couplings played in fission dynamics. In Figure 5 we plot the nonadiabatic relaxation of the S1 population from the SQC simulations for Model 1 with varied electronic couplings. The fitted decay time (from eq 20) obeys an excellent linear relationship with the electronic coupling in the log–log plot (see the inset), that is, $k_{\mathrm{S1}\to\mathrm{TT}} \propto V^{\xi}$, here $V = -V(\mathrm{S1\text{-}CT}) = -V(\mathrm{CT\text{-}TT})$. The scaling factor ξ = 2.65 is a bit great than that is predicted by either Förster or Marcus theory (ξ = 2) but smaller than that was suggested by Redfield theory (ξ = 4) for another model system.[22] Indeed the scaling factor depends on the setting of energy levels, ex. ξ = 3.25 for model 4, but relatively insensitive to the bath modeling, such as reorganization energy or characteristic frequency (see Supporting Information Figure S2). Changing one or both signs of V(S1-CT) and V(CT-TT) does not affect the dynamics at all (not shown). The change in

dx.doi.org/10.1021/ct500953r | J. Chem. Theory Comput. 2015, 11, 28–36

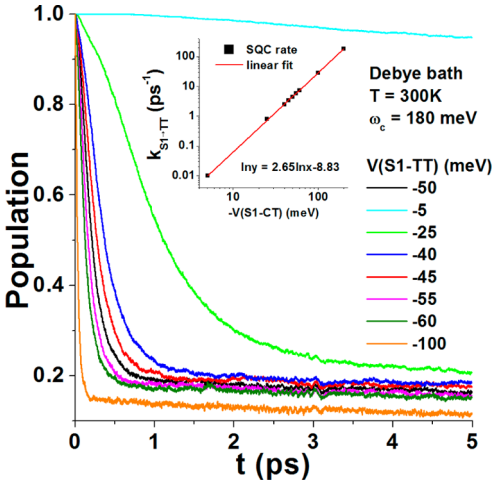

Figure 5. S1 population decay as a function of electronic couplings. Results are for Model 1 with T = 300 K, ω_c = 180 meV, and λ = 100 meV. The inset plot shows the fitted SQC rates from eq 20 (squares) and the log−log fit to these data (red line).

the magnitude for one of the coupling merely alters the dynamics quantitatively, which results in population decay between those obtained from the two different same-coupling relaxation processes (see Supporting Information Figure S3).

The results above are all for the CT-mediated mechanism, that is, the direct coupling V(S1-TT) = 0. When both the CT-mediated pathway and the direct pathway get involved, it has been shown[17,36] that quantum interference between different pathways mediates the fission dynamics in a robust way. Pathway interference can be understood from a straightforward theoretical analysis (see eq 15). Here, we apply Förster theory (eq 9) and Marcus theory (eq 10) to the initial and the final state directly (i.e., j = S1, k = TT) to predict the overall S1-TT transition rate, with the effective S1-TT coupling calculated by eq 15. Results are shown in Table 3 (labeled by Förster II and Marcus II, respectively) in comparison with the fitted decay times from the SQC simulations. Alternatively, the rate can be evaluated by the kinetic rate equations (eq 19), with the state−state rates obtained by Förster theory. The results are also listed in Table 3 (Förster III). Förster III predicts the rates on the same order as the SQC results but is unable to describe pathway interference. The sign in the direct coupling cannot be captured in Förster III since the overall rate is the classical superposition of state−state rates (proportional to the square of the corresponding coupling), which resembles quantum interference in the well-known double slit experiment. At the first glance, Forster II and Marcus II predict rates that are about 6−10 times faster than the SQC results. However, if we rescale the rates by a uniform scaling factor that sets the one with no direct coupling equal to the SQC result, both Förster II and Marcus II show excellent agreement with the simulation. This implies that pathway interference is largely attributed to the effective electronic coupling, and the deviation in the overall rate prediction may be due to the insufficient description on the global energy landscape (no intermediate state explicitly accounted). Quantum coherence in pathways is a general picture and similar results are obtained under other conditions, such as different energy levels, or different bath modeling (see Supporting Information Tables S1−S4).[17,36]

Table 3. S1 Decay Times (in fs) versus the Direct Electronic Coupling (in meV)[a]

V(S1-TT)	SQC	Förster II	Marcus II	Förster III	Förster Re	Marcus Re
−5	162	16.0	27.6	169	169	169
−3	184	17.8	30.7	192	188	188
−2	198	18.8	32.5	201	199	199
0	223	21.1	36.5	208	223	223
2	251	23.9	41.3	201	253	252
3	265	25.5	44.1	192	270	269
5	300	29.2	50.5	169	309	309

[a]Results are obtained by the fit to the SQC simulation and from different analytical approximations.

IV. CONCLUSIONS

The symmetrical quasi-classical (SQC) approach is applied to study the nonadiabatic relaxation dynamics in singlet fission. The effect of energy levels, electronic couplings and some features in bath modeling on the fission rate is investigated. The results are compared with those calculated by using other analytical approximations, namely, Förster theory, Marcus theory, and some of their variants. Förster theory predicts the rate in excellent agreement with the SQC approach for a number of different settings in energy diagram in a wide range of reorganization energy, except for the low frequency bath and/or in the downhill model (Model 2). The overestimate on the rate in the downhill model seems to be the reason why a sequential mechanism is preferred over the superexchange mechanism. Marcus theory and some of its variants are in general not as good as Förster theory since further approximations are applied. This is in consistent with the similar comparison done in recent work on the photoinduced electron transfer in molecular systems.[38−40] In our case, the SQC approach predicts a nearly linear dependence of rate on reorganization energy for the downhill model with low frequency bath at low temperature. Note that although Redfield theory seems work fine in this case, it would be invalid in the strong electronic−phonon coupling regime.

The dependence of fission dynamics on electronic couplings follows a linear relationship in the log−log plot. The scaling factor depends on energy levels but is less sensitive to bath modeling. Pathway (quantum) interference can be explained well in terms of the effective coupling between the initial and the final state based on a simple perturbation analysis. By contrast, the kinetic rate equation cannot capture the pathway interference due to the classical superposition rule. Neither Förster theory nor Marcus theory predicts the rate well in terms of the perturbed effective coupling. However, after rescaling, both are in excellent agreement with the SQC results, which advocates the idea that pathway interference origins mainly from the effective electronic coupling.

It is clear that the efficiency of singlet fission may be controlled by the design principles relying on key factors including energy levels, electronic couplings, bath modeling, or quantum coherence, which also indicates the importance of theoretical analysis. Although the approximate analytical treatments, such as Förster theory, Marcus theory or their variants, sometimes may provide quick estimates on fission rates or the effect of pathway interference (with proper rescaling), cautions must be used since the results may be misleading. Furthermore, we should keep in mind that fission dynamics is much more complicated than that a single number (rate) can quantify. For example, Förster theory is unable to

dx.doi.org/10.1021/ct500953r | J. Chem. Theory Comput. 2015, 11, 28−36

describe detailed dynamics in the nonadiabatic relaxation, such as quantum coherence. The understanding of microscopic mechanisms of singlet fission really needs real time nonadiabatic molecular dynamics simulations,[41−43] such as the efficient SQC approach we suggest here.

■ ASSOCIATED CONTENT

Supporting Information

Rate dependence on different bath type and electronic couplings, and additional details on pathway interference. This material is available free of charge via the Internet at http://pubs.acs.org.

■ AUTHOR INFORMATION

Corresponding Author

*E-mail: taogh@pkusz.edu.cn.

Notes

The authors declare no competing financial interest.

■ ACKNOWLEDGMENTS

G.T. is grateful to Professor William H. Miller for stimulating discussions and suggestions. This work was supported by Peking University Shenzhen Graduate School and Shenzhen Science and Technology Innovation Council. We also acknowledge a generous allocation of supercomputing time from the National Supercomputing Center in Shenzhen (Shenzhen Cloud Computing Center).

■ REFERENCES

(1) Smith, M. B.; Michl, J. Singlet Fission. *Chem. Rev.* **2010**, *110*, 6891−6936.

(2) Smith, M. B.; Michl, J. Recent Advances in Singlet Fission. *Annu. Rev. Phys. Chem.* **2013**, *64*, 361−386.

(3) Chan, W.-L.; Ligges, M.; Jailaubekov, A.; Kaake, L.; Miaja-Avila, L.; Zhu, X. Y. Observing the Multiexciton State in Singlet Fission and Ensuing Ultrafast Multielectron Transfer. *Science* **2011**, *334*, 1541−1545.

(4) Chan, W.-L.; Ligges, M.; Zhu, X. Y. The Energy Barrier in Singlet Fission Can Be Overcome through Coherent Coupling and Entropic Gain. *Nat. Chem.* **2012**, *4*, 840−845.

(5) Wilson, M. W. B.; A. Rao, A.; Clark, J.; Kumar, R. S. S.; Brida, D.; Cerullo, G.; Friend, R. H. Ultrafast Dynamics of Exciton Fission in Polycrystalline Pentacene. *J. Am. Chem. Soc.* **2011**, *133*, 11830−11833.

(6) Wilson, M. W. B.; A. Rao, A.; Johnson, K.; Gélinas, S.; Di Pietro, R.; Clark, J.; Friend, R. H. Temperature-Independent Singlet Exciton Fission in Tetracene. *J. Am. Chem. Soc.* **2013**, *135*, 16680−16688.

(7) Kuhlman, T. S.; Kongsted, J.; Mikkelsen, K. V.; Møller, K. B.; Sølling, T. I. Interpretation of the Ultrafast Photoinduced Processes in Pentacene Thin Films. *J. Am. Chem. Soc.* **2010**, *132*, 3431−3439.

(8) Zimmerman, P. M.; Zhang, Z.; Musgrave, C. B. Singlet Fission in Pentacene through Multi-exciton Quantum States. *Nat. Chem.* **2010**, *2*, 648−652.

(9) Sharifzadeh, S.; Darancet, P.; Kronik, L.; Neaton, J. B. Low-Energy Charge-Transfer Excitons in Organic Solids from First-Principles: The Case of Pentacene. *J. Phys. Chem. Lett.* **2013**, *4*, 2197−2201.

(10) Tiago, M. L.; Northrup, J. E.; Louie, S. G. Ab Initio Calculation of the Electronic and Optical Properties of Solid Pentacene. *Phys. Rev. B* **2003**, *67* (115212), 1−6.

(11) Cudazzo, P.; Gatti, M.; Rubio, A. Excitons in Molecular Crystals from First-Principles Many-Body Perturbation Theory: Picene versus Pentacene. *Phys. Rev. B* **2012**, *86* (195307), 1−8.

(12) Jundt, C.; Klien, G.; Sipp, B.; Le Moigne, J.; Joucla, M.; Villaeys, A. A. Exciton Dynamics in Pentacene Thin Films Studied by Pump-Probe Spectroscopy. *Chem. Phys. Lett.* **1995**, *241*, 84−88.

(13) Marciniak, H.; Fiebig, M.; Huth, M.; Schiefer, S.; Nickel, B.; Selmaier, F.; Lochbrunner, S. Ultrafast Exciton Relaxation in Microcrystalline Pentacene Films. *Phys. Rev. Lett.* **2007**, *99* (176402), 1−4.

(14) Johnson, J. C.; Reilly, T. H.; Kanarr, A. C.; van de Lagemaat, J. The Ultrafast Photophysics of Pentacene Coupled to Surface Plasmon Active Nanohole Films. *J. Phys. Chem. C* **2009**, *113*, 6871.

(15) Zimmerman, P. M.; Bell, F.; Casanova, D.; Head-Gordon, M. Mechanism for Singlet Fission in Pentacene and Tetracene: From Single Exciton to Two Triplets. *J. Am. Chem. Soc.* **2011**, *133*, 19944−19952.

(16) Chan, W.-L.; Berkelbach, T. C.; Provorse, M. R.; Monahan, N. R.; Tritsch, J. R.; Hybertsen, M. S.; Reichman, D. R.; Gao, J.; Zhu, X.-Y. The Quantum Coherent Mechanism for Singlet Fission: Experiment and Theory. *Acc. Chem. Res.* **2013**, *46*, 1321−1329.

(17) Tao, G. Electronically Non-Adiabatic Dynamics in Singlet Fission: a Quasi-Classical Trajectory Simulation. *J. Phys. Chem. C* **2014**, *118*, 17299−17305.

(18) Greyson, C.; Vura-Weis, J.; Michl, J.; Ratner, M. A. Maximizing Singlet Fission in Organic Dimers: Theoretical Investigation of Triplet Yield in the Regime of Localized Excitation and Fast Coherent Electron Transfer. *J. Phys. Chem. B* **2010**, *114*, 14168−14177.

(19) Teichen, P.; Eaves, J. D. A Microscopic Model of Singlet Fission. *J. Phys. Chem. B* **2012**, *116*, 11473−11481.

(20) Akimov, A. V.; Prezhdo, O. V. The PYXAID Program for Non-Adiabatic Molecular Dynamics in Condensed Matter Systems. *J. Chem. Theory Comput.* **2013**, *9*, 4959−4972.

(21) Akimov, A.; Prezhdo, O. V. Nonadiabatic Dynamics of Charge Transfer and Singlet Fission at the Pentacene/C60 Interface. *J. Am. Chem. Soc.* **2014**, *136*, 1599−1608.

(22) Berkelbach, T. C.; Hybertsen, M. S.; Reichman, D. R. Microscopic Theory of Singlet Exciton Fission. II. Application to Pentacene Dimers and the Role of Superexchange. *J. Chem. Phys.* **2013**, *138* (114103), 1−12.

(23) Berkelbach, T. C.; Hybertsen, M. S.; Reichman, D. R. Microscopic Theory of Singlet Exciton Fission. I. General Formulation. *J. Chem. Phys.* **2013**, *138* (114102), 1−16.

(24) Förster, T. Transfer Mechanisms of Electronic Excitation. *Discuss. Faraday Soc.* **1959**, *27*, 7−17.

(25) Marcus, R. A. Chemical and Electrochemical Electron-Transfer Theory. *Annu. Rev. Phys. Chem.* **1964**, *15*, 155−169.

(26) Fleming, G. R.; Ishizaki, A. Unified Treatment of Quantum Coherent and Incoherent Hopping Dynamics in Electronic Energy Transfer: Reduced Hierarchy Equation Approach. *J. Chem. Phys.* **2009**, *130* (234111), 1−10.

(27) Beck, M. H.; Jackle, A.; Worth, G. A.; Meyer, H. D. The Multiconfiguration Time-dependent Hartree (MCTDH) Method: A Highly Efficient Algorithm for Propagating Wavepackets. *Phys. Rep.* **2000**, *324*, 1−105.

(28) Wang, H.; Thoss, M. Multilayer Formulation of the Multi-configuration Time-Dependent Hartree Theory. *J. Chem. Phys.* **2003**, *119*, 1289−1299.

(29) Akimov, A. V.; Prezhdo, O. V. Advanced Capabilities of the PYXAID Program: Integration Schemes, Decoherence Effects, Multi-excitonic States, and Field-Matter Interaction. *J. Chem. Theory Comput.* **2013**, *10*, 789−804.

(30) Tully, J. C. Molecular Dynamics with Electronic Transitions. *J. Chem. Phys.* **1990**, *93*, 1061−1071.

(31) Meyer, H. D.; Miller, W. H. A Classical Analog for Electronic Degrees of Freedom in Nonadiabatic Collision Processes. *J. Chem. Phys.* **1979**, *70*, 3214−3223.

(32) Miller, W. H. Electronically Nonadiabatic Dynamics via Semiclassical Initial Value Methods. *J. Phys. Chem. A* **2009**, *113*, 1405−1415.

(33) Cotton, S. J.; Miller, W. H. Symmetrical Windowing for Quantum States in Quasi-Classical Trajectory Simulations. *J. Phys. Chem. A* **2013**, *117*, 7190−7194.

(34) Cotton, S. J.; Miller, W. H. Symmetrical Windowing for Quantum States in Quasi-Classical Trajectory Simulations: Application

to Electronically Non-Adiabatic Processes. *J. Chem. Phys.* **2013**, *139* (234112), 1−9.
(35) Cotton, S. J.; Igumenshchev, K.; Miller, W. H. Symmetrical Windowing for Quantum States in Quasi-Classical Trajectory Simulations: Application to Electron Transfer. *J. Chem. Phys.* **2014**, *141* (084104), 1−10.
(36) Tao, G. Bath Effect in Singlet Fission Dynamics. *J. Phys. Chem. C* **2014**, *118*, 27258−27264.
(37) Wang, H.; Thoss, M.; Sorge, K. L.; Gelabert, R.; Giménez, X.; Miller, W. H. Semiclassical Description of Quantum Coherence Effects and Their Quenching: A Forward−Backward Initial Value Representation Study. *J. Chem. Phys.* **2001**, *114*, 2562−2571.
(38) Lee, M. H.; Dunietz, B. D.; Geva, E. Calculation from First Principles of Intramolecular Golden-Rule Rate Constants for Photo-Induced Electron Transfer in Molecular Donor−Acceptor Systems. *J. Phys. Chem. C* **2013**, *117*, 23391−23401.
(39) Lee, M. H.; Geva, E.; Dunietz, B. D. Calculation from First-Principles of Golden Rule Rate Constants for Photoinduced Subphthalocyanine/Fullerene Interfacial Charge Transfer and Recombination in Organic Photovoltaic Cells. *J. Phys. Chem. C* **2014**, *118*, 9780−9789.
(40) Lee, M. H.; Dunietz, B. D.; Geva, E. Donor-to-Donor vs Donor-to-Acceptor Interfacial Charge Transfer States in the Phthalocyanine−Fullerene Organic Photovoltaic System. *J. Phys. Chem. Lett.* **2014**, *5*, 3810−3816.
(41) Tao, G.; Miller, W. H. Semiclassical Description of Electronic Excitation Population Transfer in a Model Photosynthetic System. *J. Phys. Chem. Lett.* **2010**, *1*, 891−894.
(42) Tao, G.; Miller, W. H. Time-Dependent Importance Sampling in Semiclassical Initial Value Representation Calculations for Time Correlation Functions. III. A State-Resolved Implementation to Electronically Non-Adiabatic Dynamics. *Mol. Phys.* **2013**, *111*, 1987−1993.
(43) Tao, G. Electronically Non-Adiabatic Dynamics in Complex Molecular Systems: An Efficient and Accurate Semiclassical Solution. *J. Phys. Chem. A* **2013**, *117*, 5821−5825.